CORA Cork Open Research Archive
Cartlann Taighde Oscailte Chorcaí

Title	Multifunctionalities of 2D MoS2 self-switching diode as memristor and photodetector
Authors	Dragoman, Mircea;Aldrigo, Martino;Dragoman, Daniela;Povey, Ian M.;Iordanescu, Sergiu;Dinescu, Adrian;Di Donato, Andrea;Modreanu, Mircea
Publication date	2020-09-23
Original Citation	Dragoman, M., Aldrigo, M., Dragoman, D., Povey, I. M., Iordanescu, S., Dinescu, A., Di Donato, A. and Modreanu, M. (2020) 'Multifunctionalities of 2D MoS2 self-switching diode as memristor and photodetector', Physica E: Low-dimensional Systems and Nanostructures. doi: 10.1016/j.physe.2020.114451
Type of publication	Article (peer-reviewed)
Link to publisher's version	10.1016/j.physe.2020.114451
Rights	© 2020, Elsevier B.V. All rights reserved. This manuscript version is made available under the CC BY-NC-ND 4.0 license. - https://creativecommons.org/licenses/by-nc-nd/4.0/
Download date	2024-05-03 20:21:24
Item downloaded from	https://hdl.handle.net/10468/10591

UCC
University College Cork, Ireland
Coláiste na hOllscoile Corcaigh

Journal Pre-proof

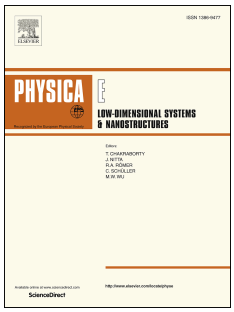

Multifunctionalities of 2D MoS_2 self-switching diode as memristor and photodetector

Mircea Dragoman, Martino Aldrigo, Daniela Dragoman, Ian M. Povey, Sergiu Iordanescu, Adrian Dinescu, Andrea Di Donato, Mircea Modreanu

PII: S1386-9477(20)31519-8

DOI: https://doi.org/10.1016/j.physe.2020.114451

Reference: PHYSE 114451

To appear in: *Physica E: Low-dimensional Systems and Nanostructures*

Received Date: 26 June 2020

Revised Date: 7 September 2020

Accepted Date: 12 September 2020

Please cite this article as: M. Dragoman, M. Aldrigo, D. Dragoman, I.M. Povey, S. Iordanescu, A. Dinescu, A. Di Donato, M. Modreanu, Multifunctionalities of 2D MoS_2 self-switching diode as memristor and photodetector, *Physica E: Low-dimensional Systems and Nanostructures*, https://doi.org/10.1016/j.physe.2020.114451.

This is a PDF file of an article that has undergone enhancements after acceptance, such as the addition of a cover page and metadata, and formatting for readability, but it is not yet the definitive version of record. This version will undergo additional copyediting, typesetting and review before it is published in its final form, but we are providing this version to give early visibility of the article. Please note that, during the production process, errors may be discovered which could affect the content, and all legal disclaimers that apply to the journal pertain.

© 2020 Published by Elsevier B.V.

Journal Pre-proof

Multifunctionalities of 2D MoS_2 self-switching diode as memristor and photodetector

Mircea Dragoman[1*], Martino Aldrigo[1], Daniela Dragoman[2,3], Ian M. Povey[4], Sergiu Iordanescu[1], Adrian Dinescu[1], Andrea Di Donato [5], Mircea Modreanu[4]

[1]National Institute for Research and Development in Microtechnologies (IMT Bucharest), Erou Iancu Nicolae Street 126A, 077190 Voluntari (Ilfov), Romania

[2]Univ. of Bucharest, Physics Faculty, P.O. Box MG-11, 077125 Bucharest, Romania

[3]Academy of Romanian Scientists, Splaiul Independentei 54, 050094 Bucharest, Romania

[4]Tyndall National Institute-University College Cork, Lee Maltings, Dyke Parade, Cork, Ireland

[5]Marche Polytechnic University, Dept. of Information Engineering, Via Brecce Bianche 60131 Ancona, Italy

Journal Pre-proof

Abstract

Self-switching diodes (SSD) were fabricated at the wafer level on a 2D few-layer MoS_2 thin film (7 monolayers) grown on a 4-inch Al_2O_3/high-resistivity silicon wafer via Chemical Vapor Deposition (CVD). We report here that MoS_2 behaves as a transparent piezoelectric material in the near infrared spectral region and as a strain-induced ferroelectric material with a measured d_{33} piezoelectric coefficient of 3-10 pm/V depending on the applied AC voltage. Moreover, we demonstrate experimentally that the SSDs behave as lateral memristors and as photodetectors in the visible spectrum, with responsivities as high as 17 A/W.

---

* Corresponding author: mircea.dragoman@imt.ro

Journal Pre-proof

1. Introduction

Self-switching diodes (SSDs) are geometrical diodes, which require no doping for rectification [1]. The SSD is in fact a side-gated field-effect transistor [2] that acts as a diode [3], the gates being shorted to the drain. We point out that there are also other types of geometric diodes where the rectification is due only to the shape of a 2D material such as graphene [4].

MoS_2 is the most studied 2D transition-metal dichalcogenide material, which has been used in various applications, such as field-effect transistors [5, 6], microwave switches [7, 8], tunable microwave circuits [9], and energy-harvesting [10]. Recently, we have shown that a 10-monolayer MoS_2 structure fabricated in the shape of a SSD is able to detect microwaves in the 0.9–10 GHz range [11]. Tens of diodes tested for RF detection proved to be square-law detectors and were used to demonstrate a MoS_2 atomically-thin microwave radio [11].

It is known that even the first radio detectors, e.g. galena detectors, were memristors [12]. Galena (PbS) is a semiconductor with the bandgap of 0.4 eV and the first rectifier had a cat-whisker configuration, memristive effects originating from charge trapping mechanisms. In this paper we explore the memristive behavior of the 2D MoS_2 by performing electrical measurements on rectifiers with the same geometry as in Ref. 11. The work reported here shows that MoS_2 SSD diodes can be lateral memristors and photodetectors, functionalities that have not yet been reported.

There are many types of 2D materials working as memristors (see the recent review [13]). The large majority of memristors are two-terminal devices and vertical structures and, where an oxide with a thickness of few nanometers is sandwiched between two metals. These vertical memristors can be integrated in a crossbar array, which is the key circuit configuration for neuromorphic applications, especially in machine learning applications such as pattern recognition [14]. However, vertical memristors suffer from several drawbacks [15], their on-state can be controlled by current compliance, i.e. by limiting the value of the current, but the off-state is far less controllable, requiring a high enough write current to form a stable filament to ensure

Journal Pre-proof

stable retention. If these problems are transferred to an array of memristors, they have a direct implication in downscaling and/or selecting the circuits which control the memristors in a cross-bar array.

On the other hand, lateral memristors such as memtransistors a three-terminal device having memristive behavior observable in the drain current-drain voltage dependence at various gate voltages, do not suffer from the above drawbacks, no electroforming is necessary and the current-voltage dependence has a hysteretic behavior that can be tuned by the gate voltage. The first memtransistors were fabricated using MoS_2 grown by CVD, which has a polycrystalline structure, the memristive effects originating from the modulation of the Schottky barrier at the source and drain of the MoS_2 backgate transistor due to migration of sulfur vacancy defects [16]. The 2D MoS_2 in the planar SSD devices presented in this paper are also polycrystalline and lateral memristors, and its memristive properties are due to unique SSD geometry and its physics.

2. Fabrication and structural characterization

We briefly explain below the growth of MoS_2 wafer and the fabrication process, which is described in detail in [11]. The MoS_2 that we use here has a nominal thickness of 7 monolayers was grown on a 4-inch 40 nm Al_2O_3/HR (high-resistivity) Si wafer and on a c-cut sapphire substrate by Chemical Vapor Deposition (CVD) process at 550 °C using $Mo(CO)_6$ (99.99% purity) and H_2S (99.99% purity) as precursors [11]. The TEM image of MoS_2 grown on Al_2O_3/HR Si shows that its thickness is 4.5 nm (see Fig. 1(a)). As will be seen further, the thickness of the 2D MoS_2 was also determined from Micro Raman Spectroscopy using a procedure describe by S.-L. Li et al. in Ref. 43 and was found to be 7 monolayers with no observed interfacial oxide. Tens of SSD diodes were fabricated by e-beam patterning and plasma oxygen etching. The diodes were subsequently protected by rectangular areas of HSQ (hydrogen silsesquioxane) patterned by an e-beam lithography process. The channel width of the diodes is 100 nm, the 30 nm Ti/200 nm Au metallic contacts being deposited by e-beam evaporation. The SEM image of the SSD “U-like” unit is displayed in Fig. 1(b). The MoS_2 SSD diode is a periodic

Journal Pre-proof

structure consisting of 11 “U-like” units, two consecutive units being separated by 70 nm. The contacts are placed 10 μm above and below the line formed by the “U-like” shapes fabricated in the MoS_2.

The atomic smoothness of the MoS_2 film was confirmed by Atomic Force Microscopy (AFM) with a built-in Piezo-Force Microscopy (PFM) functionality (Tips Nano, CSG01/Pt). The description of the settings used in the AFM and PFM techniques are reported in [17] and therefore will not be repeated here. The tip is placed in contact with the sample and oscillates due to the AC voltage applied between it and the sample. The information is recovered through a lock-in detection scheme at the resonant frequency of the whole tip-sample system.

In Fig. 2(a) we report the topography of the MoS_2 obtained by scanning a region of 100 μm×100 μm in the contact mode. PFM measurements were performed over the same region at 2 different points along a straight line (red circles in Fig. 2(a)), the average roughness and RMS of the sample surface being equal to 0.453 nm and 0.687 nm, respectively. On each point the magnitude and phase of the piezoelectric response were obtained by applying different AC voltages to the tip and a DC bias voltage in the range of +/- 10 V to polarize the sample. The DC voltage is switched off while the tip is moving from one measurement point to the other. We have observed that over those regions on which an AC or DC plus AC voltages are applied through the AFM tip, the surface topography is deformed (see the topography profiles reported in Figs. 2(b,c)) due to the piezoelectric behaviour of MoS_2 [18].

A more detailed description of the ferroelectric behaviour of MoS_2 is provided by the analysis of PFM spectroscopy curves for different values of the AC voltage amplitude applied to the tip, as illustrated in Fig. 3. Each plot of amplitude and phase was recorded by scanning the DC voltage between −10 V and + 10 V in both directions. Starting from an applied AC voltage with amplitude of around 0.5 V, we observe that both amplitude and phase have a hysteretic behaviour with a phase shift around 200 degrees, indicating the onset of ferroelectricity via strain (see Fig. 3(b)). This finding is in agreement with the fact that strain is a common means to

Journal Pre-proof

induce ferroelectricity in many materials, a recently reported example being HfO_2-based ferroelectrics [19], and is known to induce significant changes in the electronic band structure of MoS_2 [20-22] and even to induce ferromagnetism in MoS_2 with defects [23]. By applying an AC voltage with an amplitude of 0.8-1 V (see Figs. 3(d,e)), the hysteretic dependences are preserved, but the PFM phase shift approaches 360 degrees, indicating that the strain is too high for the onset of ferroelectricity, the polarization states returning to their original orientation.

The strain S_j developed in a piezoelectric material by the applied electric field E_i is described by the following matrix equation: $S_{ij} = d_{ij} E_j$ where d_j is the piezoelectric coefficient with the unit of m/V. The indices from 1 to 3 indicate components along the *x*, *y*, and *z* axis of an orthogonal coordinate system. In our case the z axis is aligned with the direction of the polarization normal to the film plane. The longitudinal piezoelectric constant d_{33} is evaluated by measuring the displacement Δz of the sample along the applied field E_3 , according to which we can write the linear relation $\Delta z = d_{33} V$. Assuming $E_3 = V/z_0$ $E_3 = V / z_0$, where z_0 is thickness of the sample and *V* the voltage applied, the strain along the normal direction can be written as: $S_3 = \Delta z / z_0 = d_{33} V / z_0$.

Since z_0 is 4.5 nm, we can estimate for the data reported in Fig.3(d) a normal strain equal to $S_3 \approx 1.406 \cdot 10^{-3}$ (strain percentage ≈ 0.14%) , whereas for the data reported in Fig.3(e), in which a different voltage is applied, we get a normal strain equal to $S_3 \approx 2.197 \cdot 10^{-3}$ (strain percentage ≈ 0.21%).

Additional and more quantitative information about the local piezoelectric behaviour of the material can be retrieved from the analysis of the piezo force response, by sweeping the amplitude of the AC voltage from close to zero up to a value beyond the local coercive voltage of the sample. A comparison between the AC-sweep curve and PFM amplitude spectroscopy is reported in Fig. 4(a). By overlapping the AC and DC voltages on the same axis the enhancement of the PFM amplitude is clearly visible in Fig. 4(a) when the AC voltage reaches 0.6-0.7 V, e.g. the value of the coercive voltage, confirming the ferroelectric behaviour of MoS_2 [24, 25]. The

Journal Pre-proof

AC-sweep curve is reported in more detail in Fig. 4(b). The piezo-response signal versus the amplitude of the AC voltage applied to the tip shows a quasi-linear dependence (up to a certain value of the voltage). As soon as the amplitude of the AC voltage is higher than the local coercive voltage, the polarization starts to switch with the same frequency as the AC voltage, leading to a strong decrease of the first harmonic response. The piezoelectric constant can be directly calculated from the slope of the linear dependence in the AC voltage [24]. By neglecting the electrostatic force and the tip-indentation effect [25], the values obtained for the piezoelectric coefficients of MoS_2 are ranging from about 3 pm/V to 10 pm/V for a DC voltage between 0 and 1 V. In ferroelectric materials, as soon as the AC amplitude is higher than the local coercive voltage, the polarization starts to switch with the same frequency as the AC voltage, leading to a decrease of the first harmonic response. However, in the range in which the applied AC voltage is around the coercive field, the polarization response of the material is enhanced and it starts being affected by some non-linear behavior, which can be intensified as the DC voltage is increased. This feature could explain the step like behavior reported in Fig. 4 (see ref [26]). The piezoelectric coefficient d_{33} is 5 pm/V in AlN and 3 pm/V in GaN [27], so that the piezoelectricity of MoS_2 is comparable or even higher than in these two semiconductors used intensively in surface-acoustic wave devices. Other results on MoS2 indicates piezoelectric coefficient d_{33} as 3.16 pm/V at 0V and 14.3 pm/V @ 0.1 GPa [28].

Raman spectra were recorded using a Renishaw Invia Reflex micro-Raman spectrometer at room temperature. The Raman mapping was collected on several sites (50 μm×50 μm, 1 μm step). The samples were excited using a CW Modu-Laser Stellar-REN laser emitting at 514.5 nm with a power of less than 0.4 mW. The reflecting microscope objective was 50X with NA = 0.75 and the excitation spot had a diameter of 1 μm. The back-scattered light was dispersed by a monochromator with a spectral resolution of 1.4 cm^{-1}, the light being detected by a charge coupled device. The typical accumulation time was 20 s. Raman shifts were calibrated using the

Journal Pre-proof

optical phonon frequency (520.5 cm^{-1}) of the silicon monocrystal. Whether the Raman spectrum of bulk MoS_2 consists of four first-order active modes: at 32 cm^{-1} (E^2_{2g}, due to vibration of an S–Mo–S layer against adjacent layers), 286 cm^{-1} (E^1_g, which is forbidden in back-scattering on a basal plane), 383 cm^{-1} (E^1_{2g}, which is an in-plane mode resulting from opposite vibration of two S atoms with respect to the Mo atom) and 408 cm^{-1} (A^1_g, associated with the out-of-plane vibration of S atoms in opposite directions) in [29-33], the asymmetric Raman peak in MoS_2 multilayers located around 454 cm^{-1} is associated to a combinational band involving a longitudinal acoustic mode (2LA(M)) and an optical mode (A_{2u}) [34].

Raman spectra were recorded using a Renishaw Invia Reflex micro-Raman spectrometer at room temperature. The Raman mapping was collected on several sites (50 μm×50 μm, 1 μm step). The samples were excited using a CW Modu-Laser Stellar-REN laser emitting at 514.5 nm with a power of less than 0.4 mW. The reflecting microscope objective was 50X with NA = 0.75 and the excitation spot had a diameter of 1 μm. The back-scattered light was dispersed by a monochromator with a spectral resolution of 1.4 cm^{-1}, the light being detected by a charge coupled device. The typical accumulation time was 20 s. Raman shifts were calibrated using the optical phonon frequency (520.5 cm^{-1}) of the silicon monocrystal. Whether the Raman spectrum of bulk MoS_2 consists of four first-order active modes: at 32 cm^{-1} (E^2_{2g}, due to vibration of an S–Mo–S layer against adjacent layers), 286 cm^{-1} (E^1_g, which is forbidden in back-scattering on a basal plane), 383 cm^{-1} (E^1_{2g}, which is an in-plane mode resulting from opposite vibration of two S atoms with respect to the Mo atom) and 408 cm^{-1} (A^1_g, associated with the out-of-plane vibration of S atoms in opposite directions) in [29-33], the asymmetric Raman peak in MoS_2 multilayers located around 454 cm^{-1} is associated to a combinational band involving a longitudinal acoustic mode (2LA(M)) and an optical mode (A_{2u}) [34].

Figure 5 illustrates the Micro Raman mapping spectra of 7ML MoS_2 deposited on the Al_2O_3/HR Si substrate (left) and characteristic Raman spectrum for 7ML MoS_2 grown on Si and c-cut sapphire substrates (right). We can observe the presence of two first-order Raman active

Journal Pre-proof

modes, at 383 cm^{-1} (E^1_{2g}) and 408 cm^{-1} (A^1_g) [34], the presence of the combinational band in MoS_2 around 454 cm^{-1} for 2D MoS_2 grown on both silicon and c-cut sapphire substrates and another peak around 520 cm^{-1} associated to the crystalline Si substrate [35]. For the 2D MoS_2 grown on Si we have employed the calibration procedure for estimating the number of MoS_2 monolayers as proposed by S.-L. Li et al. [35]. The method involved the use of the peak area ratios of MoS_2 E^1_{2g} phonon mode to Si phonon mode (520 cm^{-1}) and of MoS_2 A^1_g to Si phonon mode (520 cm^{-1}). The calculated area ratios have been found to be 1.7 and 3.2, respectively, these values corresponding to 7 monolayers of MoS_2 [35]. The observed broadening of both E^1_{2g} and A^1_g phonon modes confirms the polycrystalline nature of our 2D MoS_2 thin film and it is consistent with the presence of MoS_2 crystalline domains of about 20 nm.

3. Results and discussions

Electrical and optical measurements of SSDs have been performed at room temperature using a calibrated characterization system Keithley 4200 SCS and Agilent Cary 700 UMA spectrophotometer. The DC probes are connected to the Keithley 4200 equipment via low-noise amplifiers and located together with the probe station in a Faraday cage. We have measured all devices at different voltage sweeps, no smoothing software being employed for the experimental data reported here. In total 50 SSDs on the MoS_2 chip were measured and all were shown to exhibit an ambipolar memristive effect, as displayed in Fig. 6. Each *I-V* current-voltage dependence from Fig. 6 is formed from 500 current-voltage points which are collected during of 10 s of measurements and followed after 3 s with a new voltage sweep. We observe that the current-voltage dependence is nonlinear above a threshold voltage of about 1 V and presents a pinched hysteretic shape, which shifts to higher currents as the number of sweeps increases.

We disinguish thus the presence of a memory effect, i.e. the current dependence on its former state. All SSDs show the same memristive effect due to the geometry of the device, more precisely due to charging and discharging of surface states on the etched sidewalls of the SSD.

Journal Pre-proof

These processes occur at biases that overcome the potential barrier between surface states and the channel [36, 37]. The current-voltage characteristics differ at different sweeps since the initial value of the surface charge modifies after each sweep [37]. So, these slight shifts are due to the potential barrier which is dependent on the number of states. We have observed that memristive behavior is improving increasing the applied DC voltages., but in this case the devices are less reliable i.e. they are destroyed within a day, while applying DC voltages below 5 V produces reproducible results after 1 month. This is due to the fact that we are dealing with very tiny structures with thickness of few nm and thus very high electrical fields are applied on them and degrade their structure.

The time domain measurement of the current at + 5 V, displayed in Fig. 7, shows that the current is progressively increasing as the number of sweeps increases until it saturates and is memorized. By further increasing the number of sweeps, the current does not change, this memory state being changed only by another DC voltage applied on the SSD. This typical memristive behavior has a time constant of tens of seconds, in agreement with results reported in [36]. Similar results are obtained by applying negative DC voltages of, say, -5 V, showing nearly mirror-image curves. Therefore, these measurements are not reproduced here.

The optical transmittance of the MoS_2 film grown on sapphire (samples fabricated in the same run with those grown on 40 nm Al_2O_3/HR Si) was measured in the normal incidence configuration using an Agilent Cary 7000 UMS spectrophotometer. Figure 8 shows the optical transmittance of the MoS_2 film grown on sapphire and that of a blank sapphire substrate. We observe that the MoS_2 film has a reasonable good transparency in the visible range of the spectrum (> 50% from 550 nm, and > 75% from 700 nm) and near zero absorption in the NIR spectral range. This finding is in agreement with the low absorption rate of few-layer MoS_2 determined by the indirect bandgap nature of this semiconductor. However, MoS_2 can act as photodetector in the visible and ultraviolet spectral ranges (see, for instance, [38-41]), so we investigated the SSDs response at white light excitation. For this purpose, we illuminated the

Journal Pre-proof

SSD with a fiber optic white light source used for the microscope illumination (Motic MLC 150C) of the chuck of the Keithley 4200. The maximum power of this source is 150 W and can be adjusted at different power levels. In Fig. 9 we represented the current-voltage dependence of the SSD at different illuminations, where 100% corresponds to 150 W. We observe that the current is increasing when the power is increased and that the current-voltage dependence is nonlinear and tends to saturate at high optical power.

Assuming that the source has a cross-section with a radius of 5 cm, and that the area of the SSD is about 190 μm^2 (see [11]), the responsitivity of the device at a bias of 4 V at which the photocurrent is about 60 μA at 100% illumination is estimated at about 17 A/W. The responsivity was calculated as $R = \Delta I_D / P_{eff}$, where $P_{eff} = (A_{SSD} / A_{laser})P$, where A_{SSD} is the SSD area, A_{laser} is the area of white light illumination, and ΔI_D is the difference between currents at maximum power P and under dark conditions. Note that this responsivity is an average value over the white light spectrum, which includes the infrared region in which our few-layer MoS_2 samples do not absorb, according to Fig. 8. Even so, the obtained R value is well above the responsivities of previous vertical photodetectors containing few-layer MoS_2 [39-41], even in those with a bull eye configuration, which reach about 7.3 A/W [36], the explanation of this huge responsivity residing in the horizontal charge carrier transport in SSDs combined with the high quality of the MoS_2/Al_2O_3 interface [42]. It should be mentioned that MoS_2-based photodetectors can attain responsivities as high as 880 A/W [43], or even larger, but using monolayer MoS_2, which has a direct bandgap and hence a much larger absorption. Also, these photodetectors are made on flakes of MoS_2 monolayers, while our SSD devices are made at the wafer level. At illumination, the current of the SSD follows the switching on and off of the incident light with time constants of about 1.2 and 0.5 seconds, respectively, as can be seen from Fig. 10; the black vertical lines in the figure are a visual aid for the dependence of the optical power in time, the incident power of the light source varying between 150 W (ON state) and zero/dark condition

Journal Pre-proof

(OFF state). The rise time and decay time were obtained from the response of to rectangular excitation by fitting with exponential functions. The rise time and decay time of MoS_2 SSD photodetectors are much lower than those obtained with a MoS_2 monolayer phototransistor [43]. In the case of MoS_2 monolayer phototransistor the rise tome is 4s and decay time 9s when on the transistor are applied much higher voltages i.e. a drain voltage of 8V and a gate voltage of -70 V.

4. Conclusions

The work reported here shows that, at the wafer level, few-layer MoS_2 is piezoelectric and can undergo a ferroelectric transition due to electrically induced strain. The ability of 2D MoS_2 to undergo a reversible phase transition is important for many applications, including actuators, surface acoustic-wave devices, and haptic devices in the infrared spectrum where MoS_2 is transparent.

Here we have exploited this reversible phase transition to demonstrate functionalities of both memristors and photodetection in arrays of SSD diode devices. Furthermore, we report that the fabricated SSDs act as excellent photodetectors in the visible spectrum, with responsivity as high as 17 A/W. In conclusion, we have used MoS_2 into novel nano-devices that demonstrate resistive memory capability with potential for neuromorphic device architecture for future telecommunication and computing, as well as very-high-responsivity visible light photodetectors for mobile device applications.

Acknowledgements: The work was supported by European Union Grant H2020 825430 (NANOSMART).

Journal Pre-proof

References

[1] A. M. Song, M. Missous, P. Omonolayering, A. R. Peaker, L. Samuelson, W. Seifert, Unidirectional electron flow in a narrow semiconductor channel: A self-switching device, Appl. Phys. Lett. 83, 1881-1883 (2003).

[2] B. Hähnlein, B. Händel, J. Pezoldt, H. Töpfer, R. Granzner, F. Schwierz, Side-gate graphene field-effect transistors with high transconductance, Appl. Phys. Lett. 101, 093504 (2012).

[3] M. Åberg, J. Saijets, A. Song, M. Prunnila, Simulation and modeling of self-switching devices, Physica Scripta T114, 123 (2004).

[4] D. Dragoman, M Dragoman, Geometrically induced rectification in two-dimensional ballistic nanodevices, J. Phys. D 46, 055306 (2013).

[5] A. Sanne, R. Ghosh, A. Rai, M. N. Yogeesh, S. H. Shin, A. Sharma, K. Jarvis, L. Mathew, R. Rao, D. Akinwande, S. Banerjee, Radio frequency transistors and circuits based on CVD MoS_2, Nano Lett. 15, 5039 (2015).

[6] Y. Liu, X. Duan, Y. Huang, X. Duan, Two-dimensional transistors beyond graphene and TMDCs, Chem. Soc. Rev. 47, 6388 (2018).

[7] M. Kim, R. Ge, X. Wu, X. Lan, J. Tice, J. C. Lee, D. Akinwande, Zero-static power radio-frequency switches based on MoS_2 atomristors, Nature Communications 9, 2524 (2018).

[8] M. Dragoman, A. Cismaru, M. Aldrigo, A. Radoi, A. Dinescu, D. Dragoman, MoS_2 thin films as electrically tunable materials for microwave applications, Appl. Phys. Lett. 107, 243109 (2015).

[9] R. Cheng, S. Jiang, Y. Chen, Y. Liu, N. Weiss, H.-C. Cheng, H. Wu, Y. Huang, X. Duan, Few-layer molybdenum disulfide transistors and circuits for high-speed flexible electronics, Nature Communications 5, 5143 (2014).

Journal Pre-proof

[10] X. Zhang, J. Grajal, X. Wang, U. Radhakrishna, Y. Zhang, J. Kong, M. S. Dresselhaus, T. Palacios, MoS_2 phase-junction-based Schottky diodes for RF Electronics, IEEE/MTT-S International Microwave Symposium, Philadelphia, USA, 10-15 June, 345 (2018).

[11] M. Dragoman, M. Aldrigo, J. Connolly, Ian M. Povey, S. Iordanescu, A. Dinescu, D. Vasilache, M. Modreanu, MoS_2 radio: detecting radio-waves with a two-dimensional (2D) transition metal dichalcogenide semiconductor, Nanotechnology 31, 06LT01 (2020).

[12] G. Gandhi, V. Aggarwal, L. O. Chua, The first radios were made using memristors, IEEE Trans. Circuits and Systems 13, 8-12 (2013).

[13] L. Zhang, T. Gong, H. Wang, Z. Guo, H. Zhang, Memristive devices based on emerging two-dimensional materials beyond graphene, Nanoscale 11, 12413-12435 (2019).

[14] R. A. Nawrocki, R. M. Voyles, S. E. Shaheen, A mini review of neuromorphic architectures and implementations, IEEE Trans. Electron Dev. 63, 3819-3829 (2016).

[15] S. Slesazeck, T. Mikolajick, Nanoscale resistive switching memory devices: a review, Nanotechnology 30, 352003 (2019).

[16] V. K. Sangwan, H.-S. Lee, H. Bergeron, I. Balla, M. E. Beck, K.-S. Chen, M. C. Hersam, Multi-terminal memtransistors from polycrystalline monolayer molybdenum disulfide, Nature 554, 500-504 (2018).

[17] M. Dragoman, M. Modreanu, I. M. Povey, A. Dinescu, D. Dragoman, A. Di Donato, E. Pavoni, M. Farina, Wafer-scale very large memory windows in graphene monolayer/HfZrO ferroelectric capacitors, Nanotechnology 29, 425204 (2018).

[18] C. Cui, F. Xue, W.-J. Hu, L.-J. Li, Two-dimensional materials with piezoelectric and ferroelectric functionalities, NPJ 2D Materials and Applications 2, 18 (2018).

[19] Y. Wei, P. Nukala, M. Salverda, S. Matzen, H. J. Zhao, J. Momand, A. Everhardt, G. R. Blake, P. Lecoeur, B. J. Kooi, J. Íñiguez, B. Dkhil, B. Noheda, A rhombohedral ferroelectric phase in epitaxially strained $Hf_{0.5}Zr_{0.5}O_2$ thin films, Nature Materials 17, 1095–1100 (2018).

Journal Pre-proof

[20] N.J. Dimple, N. Jena, S. D. Behere, A. De Sarkar, The effects of different possible modes of uniaxial strain on the tunability of electronic and band structures in MoS_2 monolayer nanosheet via first-principles density functional theory, Pramana 89, 2 (2017).

[21] J. Kang, H. Sahin, F. M. Peeters, Mechanical properties of monolayer sulphides: a comparative study between MoS_2, HfS_2 and TiS_3, Phys. Chem. Chem. Phys. 17, 27742-27749 (2015).

[22] S. Yu, Q. Rice, T. Neupane, B. Tabibi, Q. Li, F. J. Seo, Piezoelectricity enhancement and bandstructure modification of atomic defect-mediated MoS_2 monolayer, Phys. Chem. Chem. Phys. 19, 24271-24275 (2017).

[23] P. Tao, H. Guo, T. Yang, Z. Zhang, Strain-induced magnetism in MoS_2 monolayer with defects, J. Appl. Phys. 115, 054305 (2014).

[24] M. Alexe, A. Gruverman, *Nanoscale Characterisation of Ferroelectric Materials, Scanning Probe Microscopy Approach*, Springer-Verlag (2004).

[25] Y. Liu, Y. Sun, W. Lu, H. Wang, Z. Wang, B. Yu, T. Li, K. Zeng, Variation of contact resonance frequency during domain switching in PFM measurements for ferroelectric materials, J. Materiomics, in press, December, (2019), https://doi.org/10.1016/j.jmat.2019.12.011

[26] Dragan Damjanovic,Ferroelectric, dielectric and piezoelectric properties of ferroelectric thin films and ceramics" Rep. Prog. Phys. 61 1267–1324 (1998).

[27] C. M. Lueng, H. L. W. Chan, C. Surya, C. L. Choy, Piezoelectric coefficient of aluminum nitride and gallium nitride, J. Appl. Phys. 88, 5360-5363 (2000)

[28] M. K. Mohanta, A Rawat, N. Jena Dimple, R. Ahammed, and A De Sarkar**,** Interfacing boron monophosphide with molybdenum Disulfide for an ultrahigh Performance in thermoelectrics, two-Dimensional excitonic solar cells, and nanopiezotronics" ACS Appl. Mater. Interfaces, 12, 2, 3114-3126 (2020)

[29] A. G. Bagnall, W. Y. Liang, E. A. Marseglia, B. Welber, Raman studies of MoS_2 at high pressure, Physica 99B, 343-346 (1980).

Journal Pre-proof

[30] M. Viršek, A. Jesih, I. Miloševic, M. Damnjanovic´, M. Remškar, Raman scattering of the MoS_2 and WS_2 single nanotubes, Surf. Sci. 601, 2868-2872 (2007).

[31] P. Budania, P. Baine, J. Montgomery, C. McGeough, T. Cafolla, M. Modreanu, D. McNeill, N. Mitchell, G. Hughes, P. Hurley, Long-term stability of mechanically exfoliated MoS_2 flakes, MRS Communications 7, 813-818 (2017).

[32] P. Budania, P. T. Baine, J. H. Montgomery, D. W. McNeill, S. J. N. Mitchell, M. Modreanu, P. K. Hurley, Effect of post-exfoliation treatments on mechanically exfoliated MoS_2, Materials Research Express 4, 025022 (2017).

[33] P. A. Bertrand, Surface-phonon dispersion of MoS_2, Phys. Rev. B 44, 5745-5749 (1991).

[34] H. Li, Q. Zhang, C. Chong, R. Yap, B. Kang Tay, T. Hang, T. Edwin, A. Olivier, D. Baillargeat, From bulk to monolayer MoS_2: evolution of Raman scattering, Adv. Funct. Mater. 22, 1385–1390 (2012).

[35] C. Smit, R. A. C. M. M. van Swaaij, H. Donker, A. M. H. N. Petit, W. M. M. Kessels, M. C. M. van den Sanden, Determining the material structure of microcrystalline silicon from Raman spectra, J. Appl. Phys. 94, 3582-3588 (2003).

[36] A. M. Song, M. Missous, P. Omonolayering, I. Maximov, W. Seifert, L. Samuelson, Nanometer-scale two-terminal semiconductor memory operating at room temperature, Appl. Phys. Lett. 86, 042106 (2005).

[37] I. Iñiguez-de-la-Torre, T. González, D. Pardo, J. Mateos, Hysteresis phenomena in nanoscale rectifying diodes: a Monte Carlo interpretation in terms of surface effects, Appl. Phys. Lett. 91, 063504 (2007).

[38] A. Sourav, Z. Li, Z. Huang, V. D. Botcha, C. Hu, J.-P. Ao, Y. Peng, H.-C. Kuo, J. Wu, X. Liu, K.-W. Ang, Large-scale transparent molybdenum disulfide plasmonic photodetector using bull eye structure, Adv. Optical Mater. 2018, 1800461 (2018).

Journal Pre-proof

[39] W. Choi, M. Y. Cho, A. Konar, J. H. Lee, G.-B. Cha, S. C. Hong, S. Kim, J. Kim, D. Jena, J. Joo, S. Kim, High-detectivity multilayer MoS_2 phototransistors with spectral response from ultraviolet to infrared, Adv. Mater. 24, 5832-5836 (2012).

[40] D.-S. Tsai, K.-K. Liu, D.-H. Lien, M.-L. Tsai, C.-F. Kang, C.-A. Lin, L.-J. Li, J.-H. He, Few-layer MoS_2 with high broadband photogain and fast optical switching for use in harsh environments, ACS Nano 7, 3905-3911 (2013).

[41] B. P. Majee, S. Mishra, R. K. Pandey, R. Prakash, A. K. Mishra, Multifunctional few-layer MoS_2 for photodetection and surface-enhanced Raman spectroscopy application with ultrasensitive and repeatable detectability, J. Phys. Chem. C 123, 18071-18078 (2019).

[42] H. Bergeron, V. K. Sangwan, J. J. McMorrow, G. P. Campbell, I. Balla, X. Liu, M. J. Bedzyk, T. J. Marks, M. C. Hersam, Chemical vapor deposition of monolayer MoS_2 directly on ultrathin Al2O3 for low-power electronics, Appl. Phys. Lett. 110, 053101 (2017).

[43] O. Lopez-Sanchez, D. Lembke, M. Kayci, A. Radenovic, A. Kis, Ultrasensitive photodetectors based on monolayer MoS_2, Nature Nanotechnology 8, 497-501 (2013)

Journal Pre-proof

Journal Pre-proof

Figure captions

Fig. 1 (a) TEM of image of the MoS_2/Al_2O_3/HR Si substrate. The MoS_2 thickness is equal to 7 monolayers ×0.65 nm = 4.5 nm, (b) SEM image of the SSD unit.

Fig. 2 (a) Topography of MoS_2 obtained by AFM, and two profiles acquired (b) along the red dotted line connecting the points of measurements (red circles) and (c) along the direction normal to this line.

Fig. 3 Piezo-Force amplitude and phase curves obtained for the following values of the AC voltage applied to the tip during PFM spectroscopy: (a) 0.1 V, (b) 0.5 V, (c) 0.6 V, (d) 0.8 V, (e) 1 V, and (f) 1.5 V.

Fig. 4 (a) Comparison between the AC-sweep curve and PFM amplitude spectroscopy. The PFM amplitude plots are obtained by sweeping the DC voltage between +/- 10 V and applying to the tip an AC voltage with an amplitude of 0.5 V. Alternatively, the AC-sweep curve is recorded by changing the amplitude of AC voltage in the range between 0.1 V -1.5 V for different DC voltages V_{DC1} = 0 V, V_{DC2} = 0.5 V, V_{DC3} = 1 V. (b) Evaluation of the piezoelectric coefficient of MoS_2 for different applied DC voltages (V_{DC1}, V_{DC2}, V_{DC3}). The coefficients are computed from the slope of the linear dependence in V_{AC}.

Fig. 5 (a) micro Raman 3D imaging of 7-monolayer MoS_2 deposited on Al_2O_3/HR Si substrate (left) (b) the characteristic Raman spectrum 7-monolayer MoS_2 grown on Al_2O_3/HR Si and on c-cut sapphire. The phonon mode for the Si substrate is also observed at around 520 cm^{-1}.

Fig. 6 Current-voltage dependences at various sweeps. Inset: the same curves for both polarities.

Fig. 7 Current-time dependences at various sweeps for a DC voltage of +5 V.

Fig. 8 Optical transmittance of 7-monolayer MoS_2 grown on sapphire substrate and the optical transmittance of a blank sapphire substrate

Fig. 9 Current-voltage dependences at various optical powers indicated as percentages of the maximum power of 150 W.

Journal Pre-proof

Fig. 10 Current-time dependence at switching on and off the optical power when the SSD is biased at 4 V.

Journal Pre-proof

Journal Pre-proof

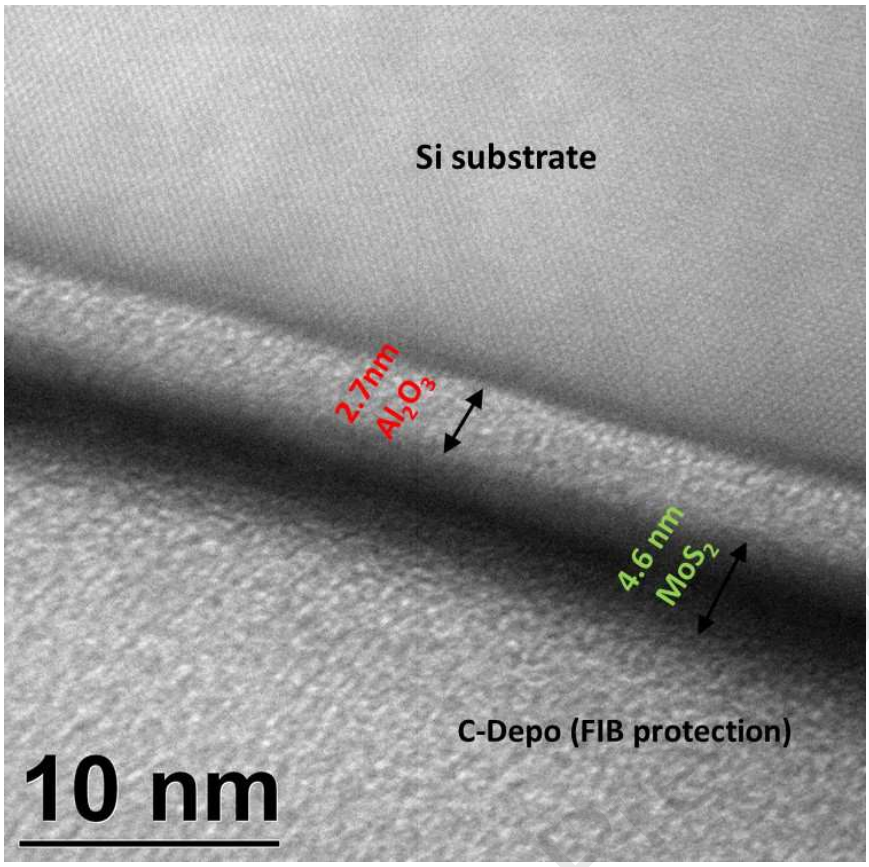

(a)

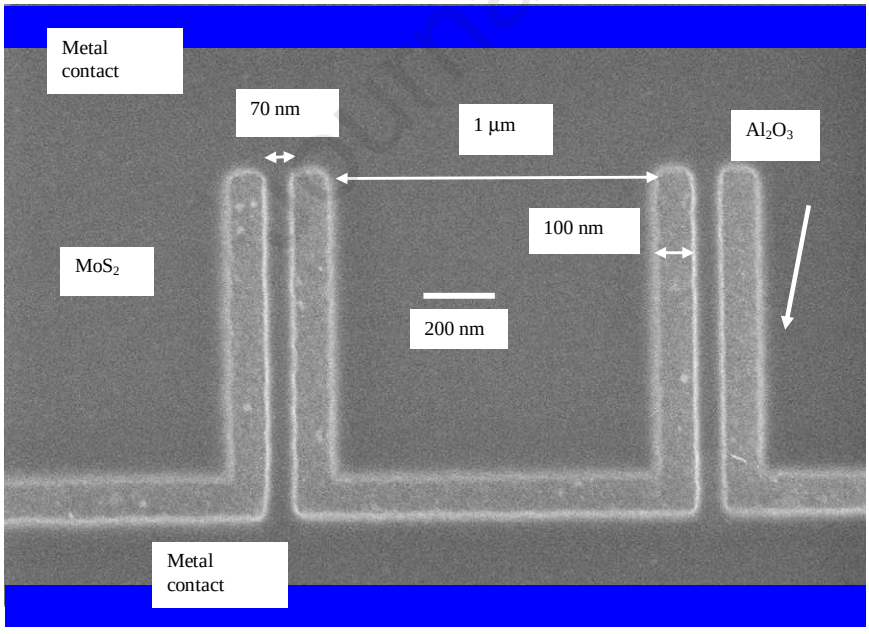

(b)

Fig. 1

Journal Pre-proof

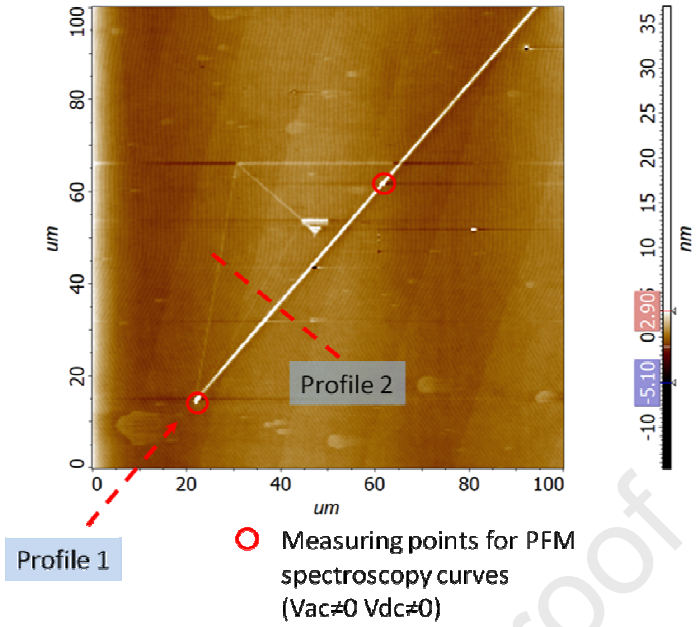

(a)

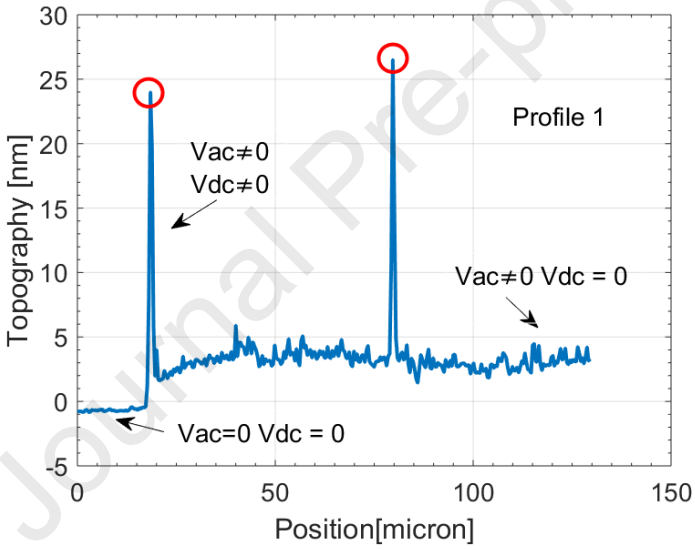

(b)

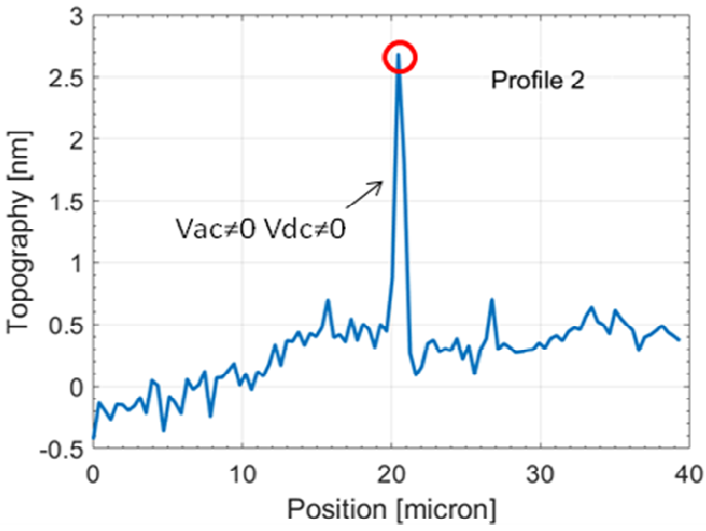

(c)

Fig. 2

Journal Pre-proof

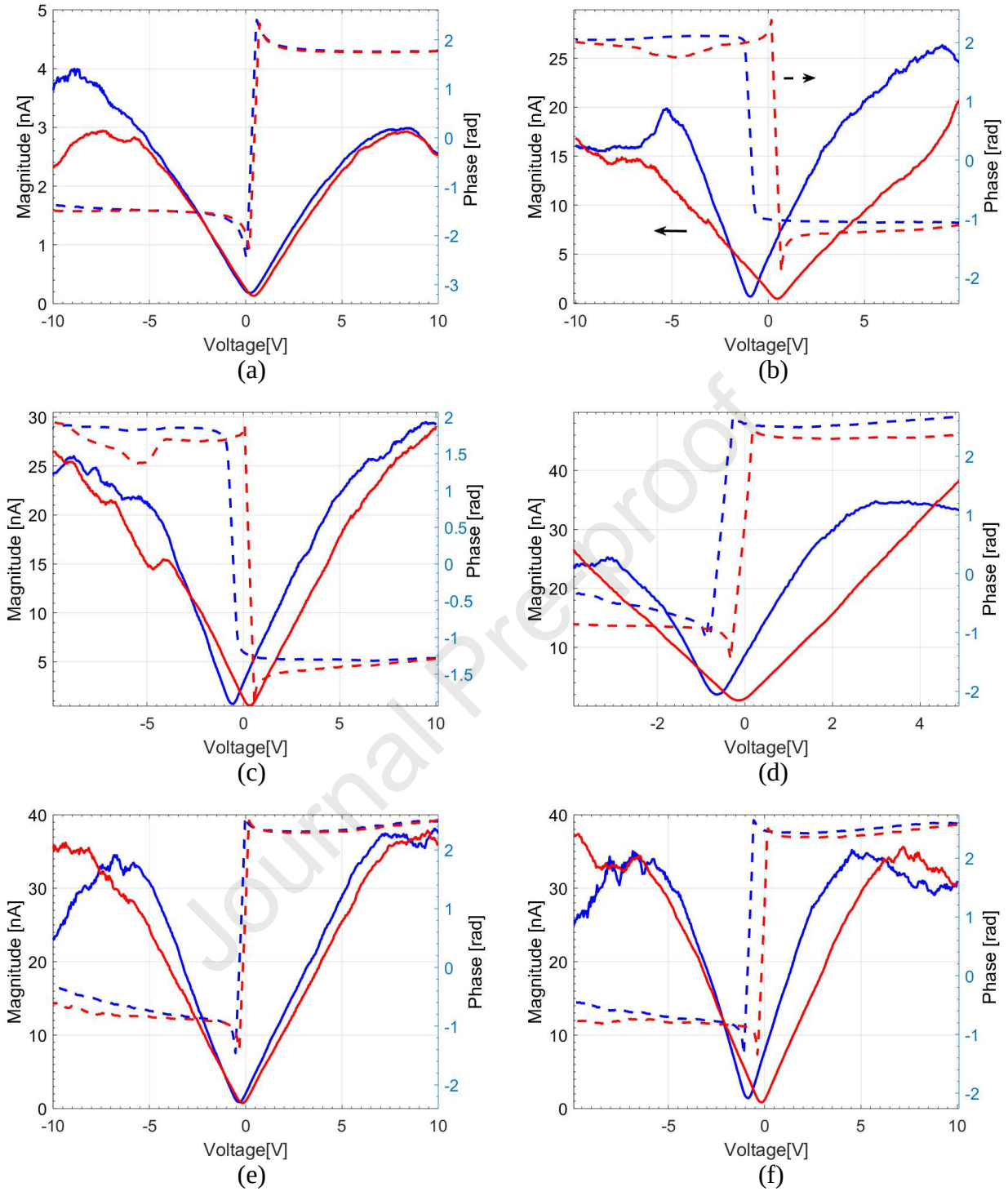

Fig. 3

Journal Pre-proof

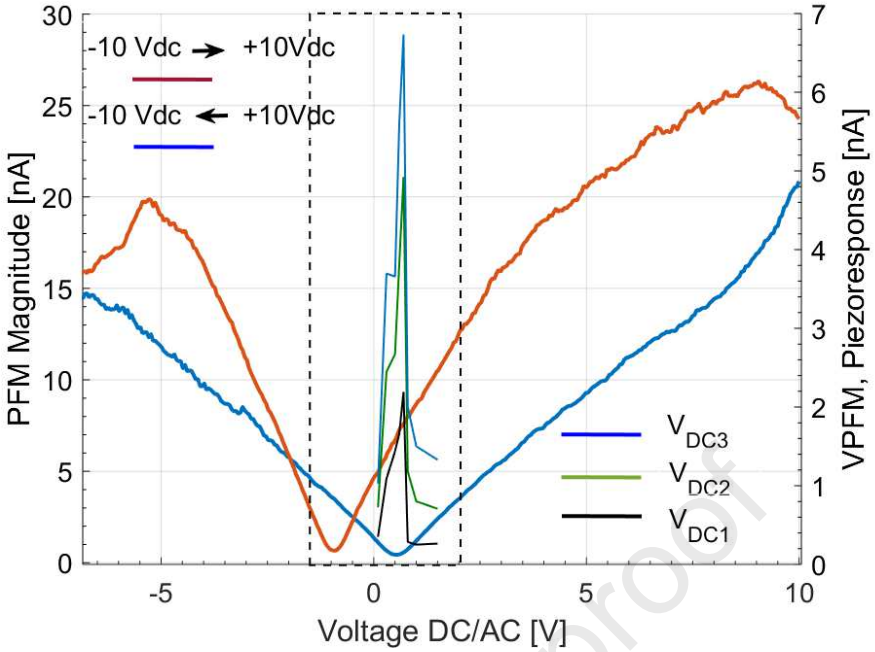

(a)

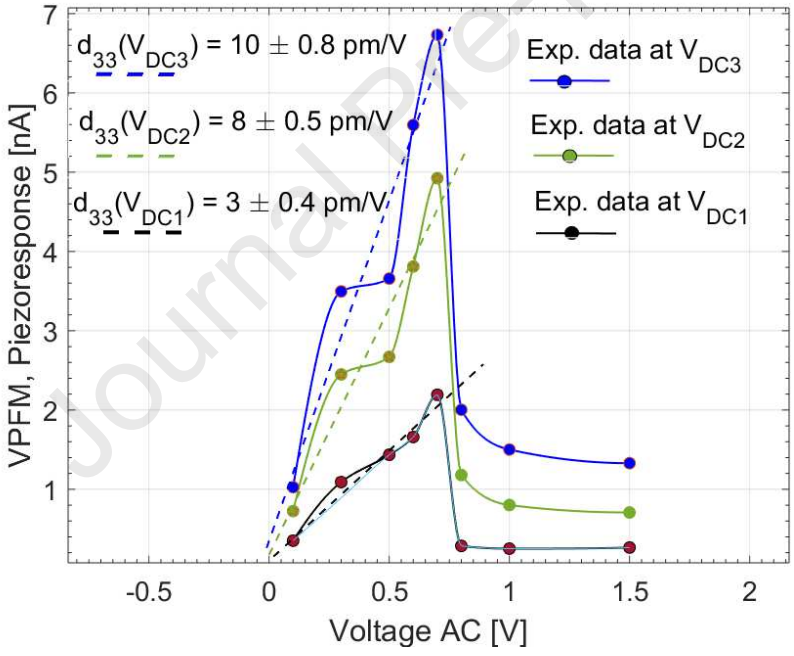

(b)

Fig. 4

Journal Pre-proof

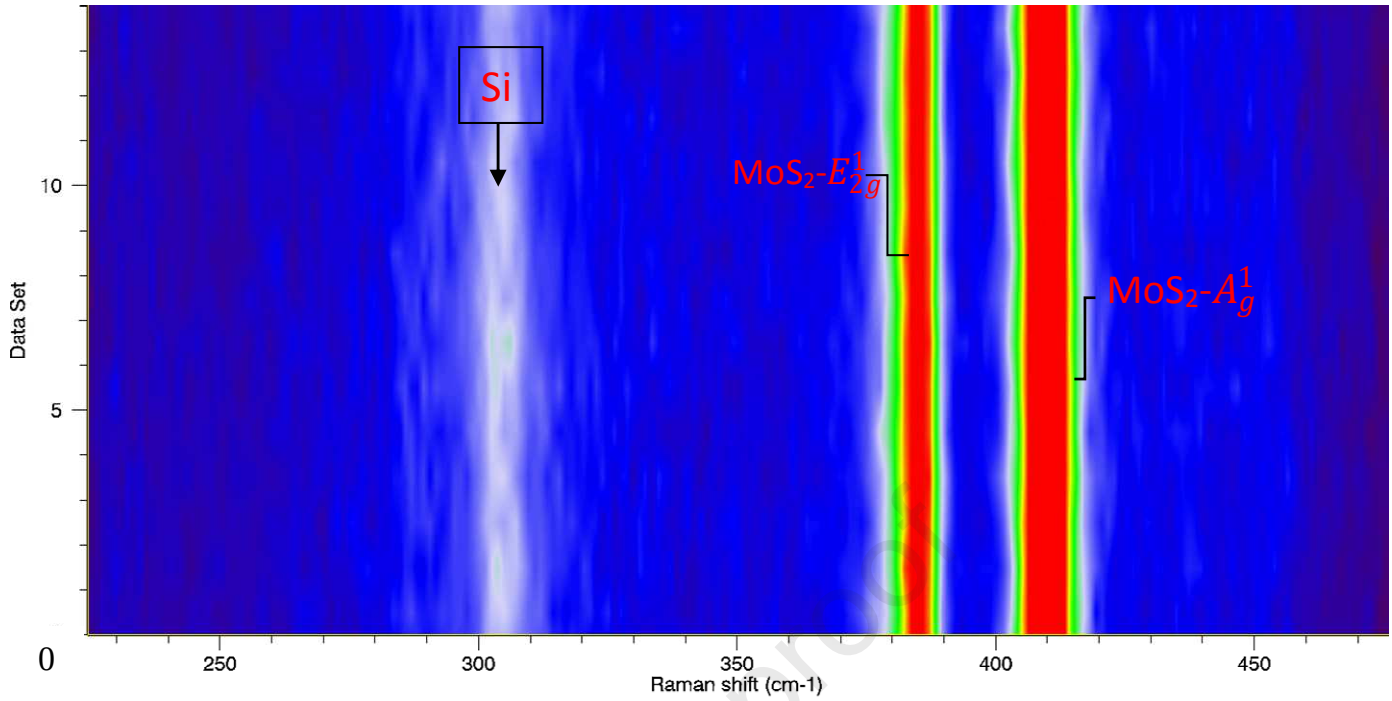

(a)

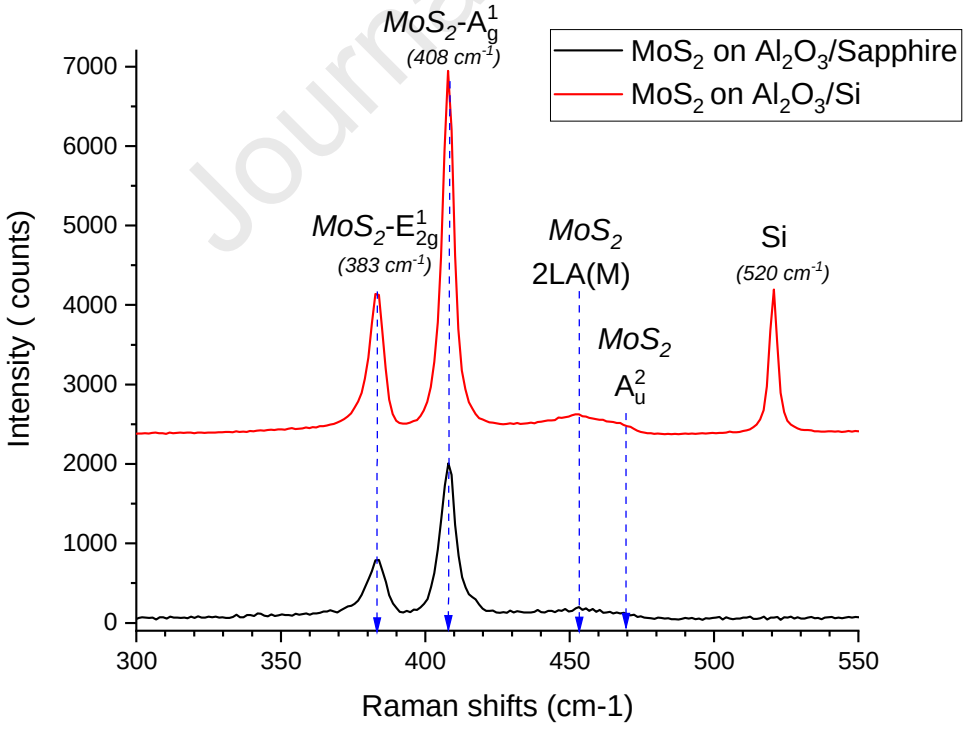

(b)

Fig. 5

Journal Pre-proof

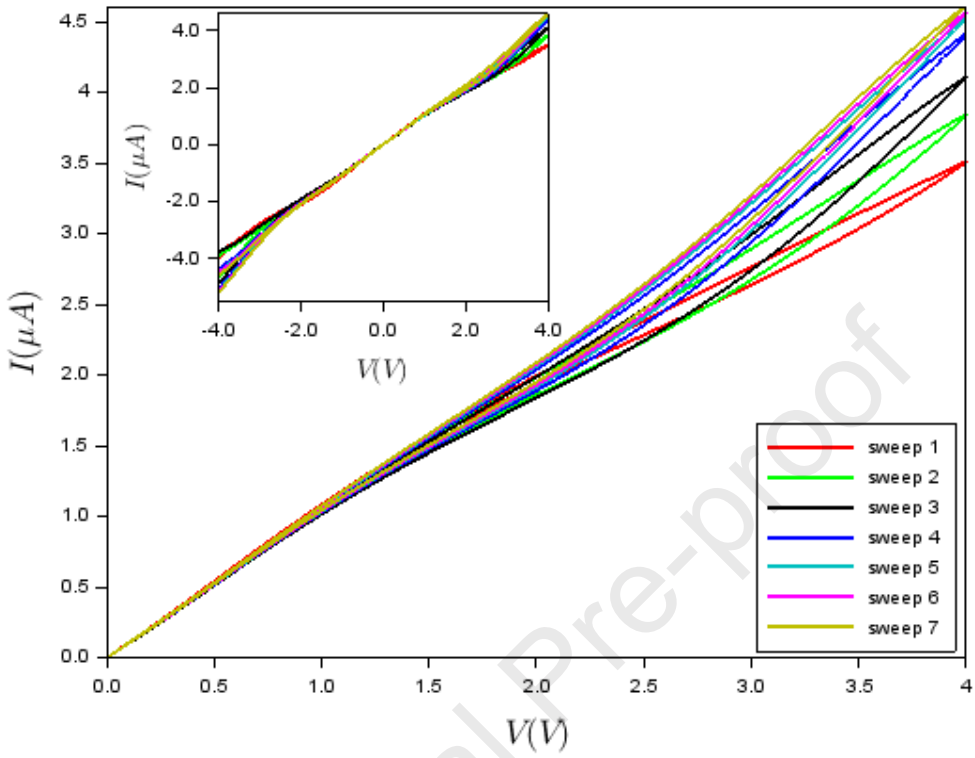

Fig. 6

Journal Pre-proof

Journal Pre-proof

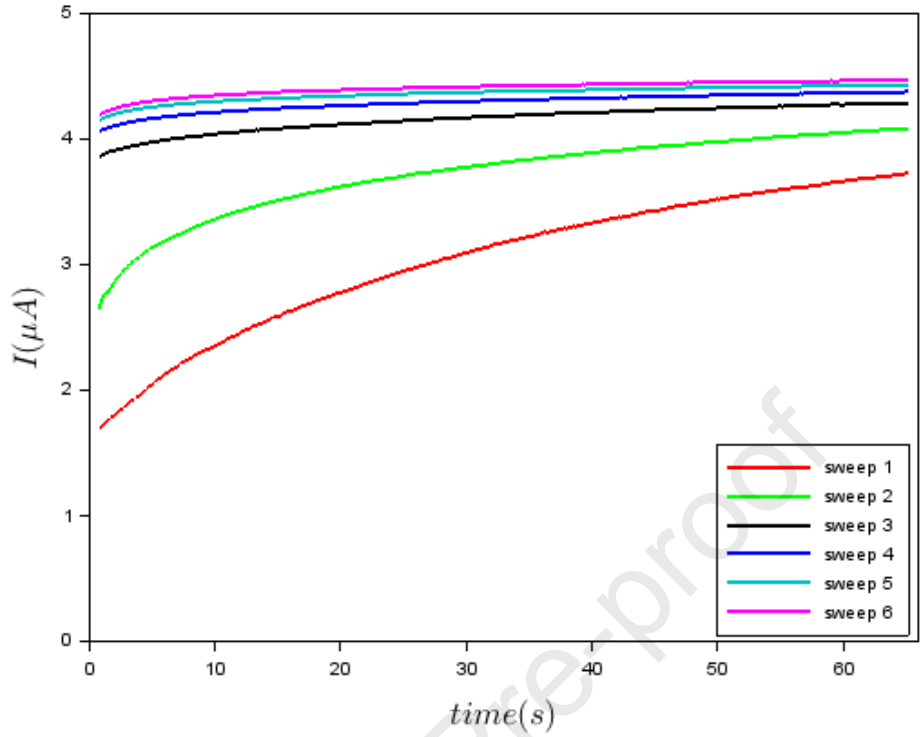

Fig. 7

Journal Pre-proof

Journal Pre-proof

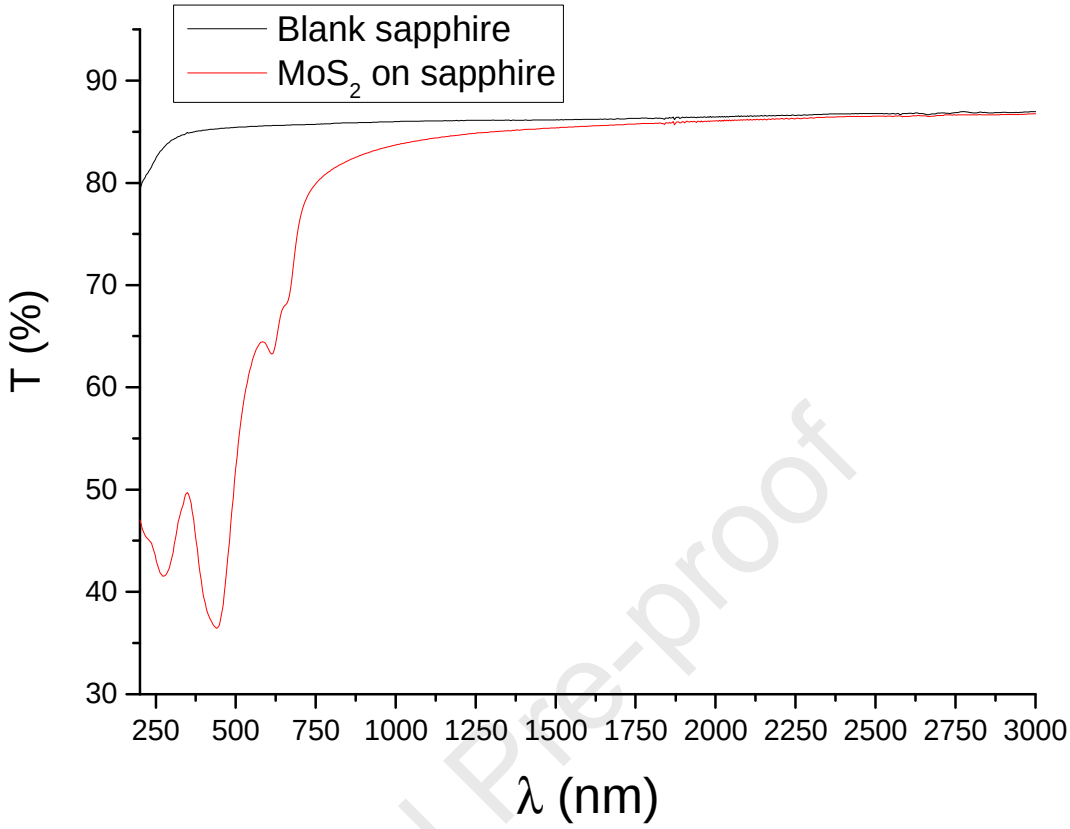

Fig. 8

Journal Pre-proof

Journal Pre-proof

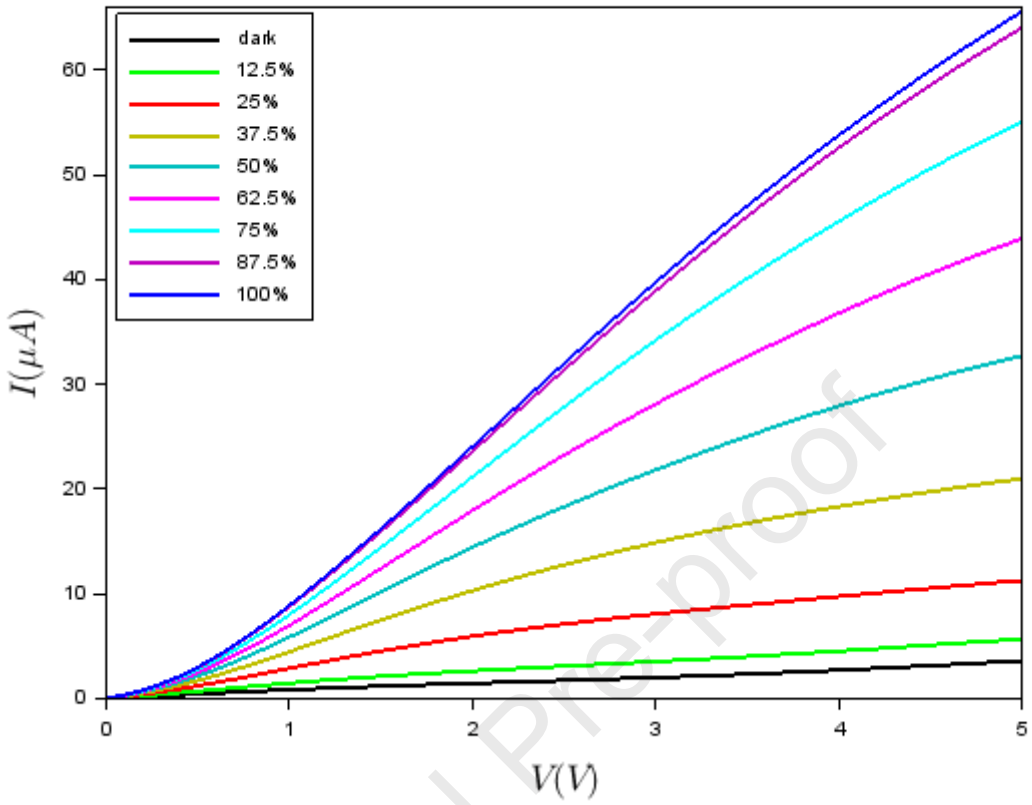

Fig. 9

Journal Pre-proof

Journal Pre-proof

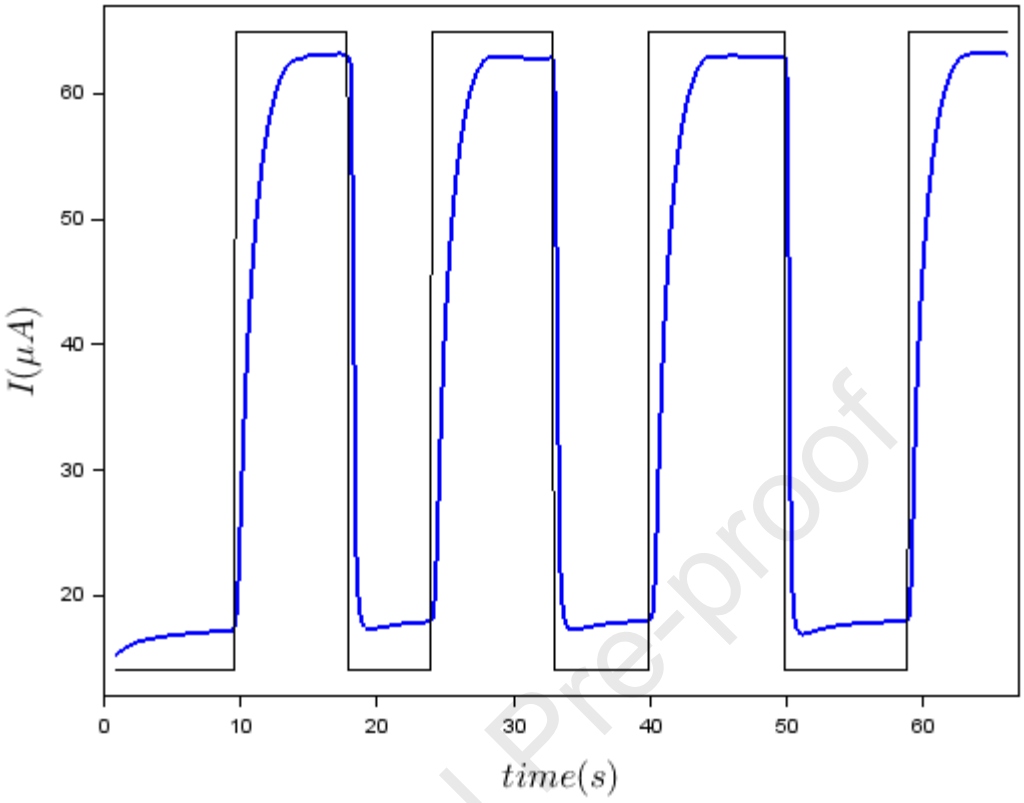

Fig. 10

Journal Pre-proof

Journal Pre-proof

The authors have contributed equally to this research work.

Journal Pre-proof

Journal Pre-proof

Declaration of interests

X☐ The authors declare that they have no known competing financial interests or personal relationships that could have appeared to influence the work reported in this paper.

☐The authors declare the following financial interests/personal relationships which may be considered as potential competing interests:

Journal Pre-proof